Available online at www.sciencedirect.com
SCIENCE DIRECT®
C. R. Physique 7 (2006) 233–243
COMPTES RENDUS PHYSIQUE
http://france.elsevier.com/direct/COMREN/

High power fiber lasers and amplifiers/Lasers et amplificateurs à fibre de puissance

High power multimode fiber amplifier with wavefront reshaping for high beam quality recovery

Laurent Lombard [a,*], Arnaud Brignon [a], Jean-Pierre Huignard [a], Éric Lallier [a], Gaëlle Lucas-Leclin [b], Patrick Georges [b], Gilles Pauliat [b], Gérald Roosen [b]

[a] *Thales Research and Technology–France, RD 128, 91767 Palaiseau, France*
[b] *Laboratoire Charles-Fabry de l'institut d'optique, du CNRS, et de l'université Paris Sud, centre universitaire, bâtiment 503, 91403 Orsay, France*

Available online 17 April 2006

Abstract

The increase in fiber laser and amplifier output power is limited by nonlinear effects and material damage due to the high power density, especially in pulsed operation. Output powers of several hundreds watts have recently been achieved with large-mode-area quasi-singlemode fibers. To further increase the core diameter, an original alternative approach consists in correcting the beam profile after a multimode fiber amplifier by a nonlinear beam cleanup method. We report the conversion of a multimode and depolarized output beam of a highly multimode diode-pumped Yb-doped fiber amplifier to a diffraction limited, linearly polarized beam by two original beam cleanup methods:

• the first converts the multimode beam to a singlemode beam using self-referencing two wave mixing process in an infrared sensitive photorefractive crystal (Rh:$BaTiO_3$). With this setup, up to 11.6 W singlemode output is achieved with a 78% multimode to singlemode photorefractive conversion efficiency,

• the second converts a multimode beam into a singlemode beam by use of the Brillouin effect in a multimode gradient-index (GI) fiber with a self-aligned loop geometry. A preliminary conversion from a $M^2 = 6.5$ beam into a $M^2 = 1.3$ beam with 31% efficiency is reported. ***To cite this article: L. Lombard et al., C. R. Physique 7 (2006).***

Résumé

Méthodes non linéaires de remise en forme de faisceaux pour amplificateur de puissance à fibre multimode. Le développement récent des fibres à large cœur quasi-monomodes a permis une montée en puissance rapide des lasers à fibre. En effet, l'utilisation d'un gros cœur permet de limiter les effets non linéaires indésirables et d'augmenter les seuils de dommage. Afin de poursuivre la montée en puissance, nous avons exploré une voie originale utilisant des fibres amplificatrices multimodes suivies d'interactions non linéaires de remise en forme. Nous reportons ici la conversion d'un faisceau dépolarisé et multimode, issu d'un amplificateur à fibre dopée Ytterbium à très large cœur, vers un faisceau polarisé linéairement et limité par la diffraction par deux méthodes non linéaires de nettoyage de faisceau originales (beam cleanup) :

• le premier réalise la remise en forme par mélange à deux ondes auto-référencé dans un cristal photoréfractif de Rh:$BaTiO_3$. Un faiseau limité par la diffraction et de puissance 11,6 W avec une efficacité de conversion dans le cristal de 78 %,

• le second réalise la conversion du faisceau multimode vers un faisceau monomode par rétrodiffusion Brillouin stimulée (SBS) dans une cavité Brillouin auto-alignée contenant une fibre multimode à gradient d'indice. Une conversion préliminaire d'un faisceau

* Corresponding author.
E-mail address: Laurent.Lombard@onera.fr (L. Lombard).

1631-0705/$ – see front matter
doi:10.1016/j.crhy.2006.02.010

de $M^2 = 6{,}5$ vers un faisceau de $M^2 = 1{,}3$ est reportée avec une efficacité de 31 %. ***Pour citer cet article : L. Lombard et al., C. R. Physique 7 (2006).***

Keywords: High power laser; Fiber amplifier; Multimode fiber; Beam cleanup; Photorefractive effect; Stimulated Brillouin scattering; Phase conjugation

Mots-clés : Laser de puissance ; Amplificateur à fibre ; Fibre multimode ; Nettoyage de faisceau ; Effet photoréfractif ; Diffusion Brillouin stimulée ; Conjugaison de phase

1. Introduction

The recent development of quasi-singlemode large mode area fibers has led to a quick rise in fiber laser power. Indeed, the large core prevents nonlinear effects and increases damage threshold. In order to further increase the core diameter, we propose an alternative approach using a very large core multimode fiber amplifier followed by a nonlinear beam cleanup interaction to restore a diffraction limited beam profile as indicated in Fig. 1. Two concepts have been studied and are presented here.

Beam quality is restored in Section 2 by self-referencing two-wave mixing in a Rh:$BaTiO_3$ photorefractive crystal. The photorefractive two-wave mixing beam cleanup interaction has been validated in previous works in visible light [1,2] after a depolarizer [3], and at 1064 nm after an aberrator [4,5]. Self-referencing two-wave mixing [6] is an improved version of this technique and the resulting mode converter can change any depolarized, aberrated and coherent laser beam into a diffraction-limited beam. Here this mode converter is applied to a diode pumped multimode Yb-doped fiber amplifier.

The second technique, described in Section 3, is a result of a detailed theoretical and experimental study of stimulated Brillouin backscattering (SBS) in multimode fibers [7]. It is well known that both phase conjugation and beam cleanup behavior are observed by SBS in multimode fibers, but the reasons why each effect occur are not clear. The study outlines the conditions in which phase conjugation (short step-index fibers) or beam cleanup (gradient-index fibers) are more likely to occur. An original geometry, a self-aligned gradient-index fiber Brillouin cavity, is proposed and experimentally demonstrated with the same diode pumped multimode Yb-doped fiber amplifier.

2. Beam cleanup by two-wave-mixing in a photorefractive crystal

In this section, we first describe the principle of two-wave mixing beam cleanup in a photorefractive crystal and the infrared sensitive Rh:$BaTiO_3$ crystal. Then the self-referencing two-wave mixing beam cleanup is presented and applied to a multimode fiber amplifier.

2.1. Principle of two-wave-mixing beam cleanup

Diffusion-type photorefractive materials allow energy transfer between two coherent beams by interference-induced index grating [8]. The photorefractive effect is a phenomenon in which the local index of refraction is changed

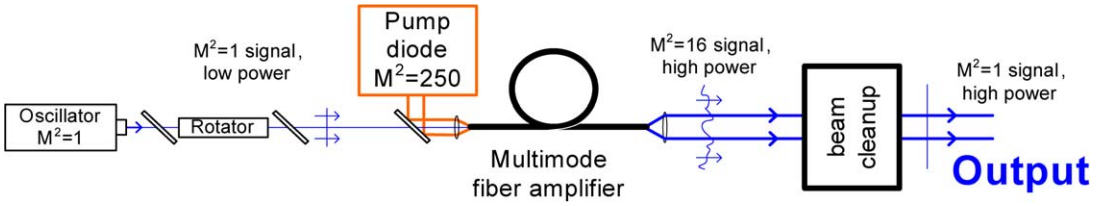

Fig. 1. Master oscillator and multimode fiber amplifier with beam reshaping setup. The master oscillator low-power high-quality output beam is amplified to a low-quality high-power beam. The last is converted to a high-quality, high-power reshaped output beam.

Fig. 1. Oscillateur maître et fibre amplificatrice multimode avec système de remise en forme. Le faisceau monomode spatial issu de l'oscillateur maître est amplifié et dégradé dans l'amplificateur et retrouve son aspect monomode après la remise en forme.

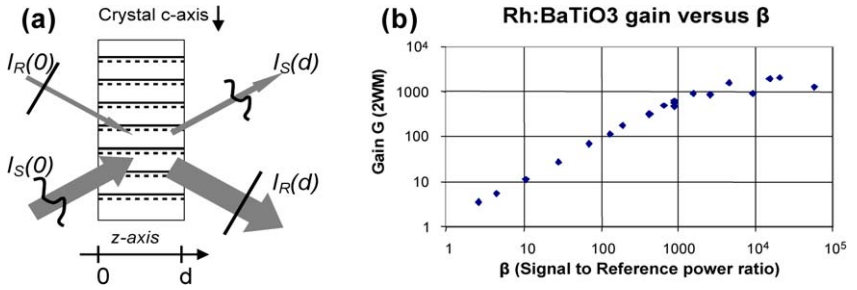

Fig. 2. (a) Two wave mixing process in a photorefractive crystal. $I_R(z)$, $I_S(z)$: intensities of beams R and S along the propagation. Continuous lines: maxima of the interference pattern. Dashed lines: maxima of the shifted index pattern; (b) measured photorefractive gain in a two wave mixing experiment as a function on incident beams intensity ratio.

Fig. 2. (a) Mélange à deux ondes dans un cristal photoréfractif. $I_R(z)$, $I_S(z)$: intensités des faisceaux R et S le long de l'axe, lignes continues : maxima de la figure d'interférence, lignes pointillées : maxima de la figure d'interférence décalée ; (b) gain photoréfractif mesuré dans une expérience de mélange à deux ondes en fonction du rapport d'intensité des faisceaux incidents.

by the spatial variation of light intensity. It arises from optically-generated charge carriers which migrate when the crystal is exposed to a spatially varying pattern of illumination. In case of diffusion-type photorefractive crystals such as $BaTiO_3$, the charge carriers are mostly generated where light is intense and then diffuse all over the crystal, leaving charge defects. This space-charge separation gives rise to a strong space-charge field that induces refractive index change by Pockel's effect.

In the case of an interference pattern between two coherent beams in the medium, the induced refraction index pattern acts as a volume diffraction grating. This is the two-wave mixing interaction: the two beams diffract on this grating along each other. Furthermore, the index pattern is shifted by a quarter wave in the direction defined by the crystal c-axis orientation (see Fig. 2(a)). In this direction the diffraction is phase-matched and S gets cumulatively diffracted along R. Thus the intensity of S is transferred to R. This effect is shown in Fig. 2(a) and expressed in the coupled equations (1) where I_R, I_S are beam intensities, Γ is the photorefractive gain coefficient (cm^{-1}) and α is the absorption coefficient (cm^{-1}).

$$\frac{\mathrm{d}I_S}{\mathrm{d}z} = -\Gamma \frac{I_S I_R}{I_S + I_R} - \alpha I_S; \qquad \frac{\mathrm{d}I_R}{\mathrm{d}z} = \Gamma \frac{I_S I_R}{I_S + I_R} - \alpha I_R \tag{1}$$

After a propagation in a crystal with a thickness d, beam R experiences an intensity gain G given by (2) where β is the reference to signal intensity ratio:

$$G = \frac{I_R(d)}{I_R(0)} = \frac{\beta + 1}{\beta + \mathrm{e}^{\Gamma d}} \cdot \mathrm{e}^{(\Gamma - \alpha)d}; \qquad \beta = \frac{I_S(0)}{I_R(0)} \tag{2}$$

The wavefront of the two beams are unaffected in the interaction: S transfers its energy and not its phase to R. This remarkable property allows the two-wave mixing beam cleanup. As shown in Fig. 2(a), a low-power singlemode beam R is mixed with a coherent high power multimode beam S, so that the index grating diffracts the high-power beam S along the singlemode beam R with the phase characteristics of R. The intense and aberrated beam S is diffracted to a singlemode intense beam R. In other words, photorefractive two-wave mixing acts as a nonlinear spatial mode converter [4].

2.2. A $Rh:BaTiO_3$ photorefractive crystal for 1 μm beam cleanup

The crystal used in the experiment is a $Rh:BaTiO_3$ crystal.[1] This crystal has a 'roof shape' to prevent any parasitic oscillation arising from beam fanning [9]. The 8×8 mm^2 input and output faces are antireflection coated and are cut at 45° from the crystal c-axis. This c-axis lies in the horizontal plane, plane of the incident polarizations, in order to access large photorefractive gains. The crystal thickness is 3 mm. The photorefractive gain, defined as G in Eq. (2), was measured in a simple two-wave mixing experiment as a function of the input power ratio β (see Fig. 2(b)). The

[1] From D. Rytz, FEE GmbH, Germany. Rh doping concentration is 1000 ppm in the melt.

maximum measured gain $G_{\max}$ is 2000, which corresponds to a photorefractive gain coefficient Γ of 24.6 cm^{-1}. With the crystal used in this experiment, both beam polarizations must be in the same plane as the crystal c-axis in order to access maximum efficiency.

2.3. Experimental setup

Fig. 4 shows the self-referencing two-wave mixing technique applied to a diode pumped multimode-Yb-doped-fiber amplifier. A CW master oscillator (Nd:YAG NPRO laser, 500 mW @ 1.06 μm, spatially and spectrally single-mode) is amplified in a multimode fiber amplifier. The amplifier uses a double clad fiber[2] with a 55 μm diameter (NA = 0.19) Yb-doped signal core (6500 mol ppm Yb_2O_3) and a 340/400 μm diameter (NA = 0.38) D-shaped pump core. A picture of the fiber is shown in Fig. 3.

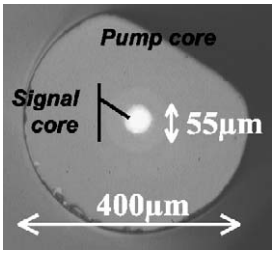

Fig. 3. Fibre used in the experiment, with a Yb-doped signal core (55 μm diameter, 0.19 NA) and a D-shaped pump core (400 μm diameter, 0.39 NA).
Fig. 3. Fibre utilisée, avec un coeur signal dopé Yb (diamètre 55 μm, ouverture 0,19) et un coeur pompe en forme de D (diamètre 400 μm, ouverture 0,39).

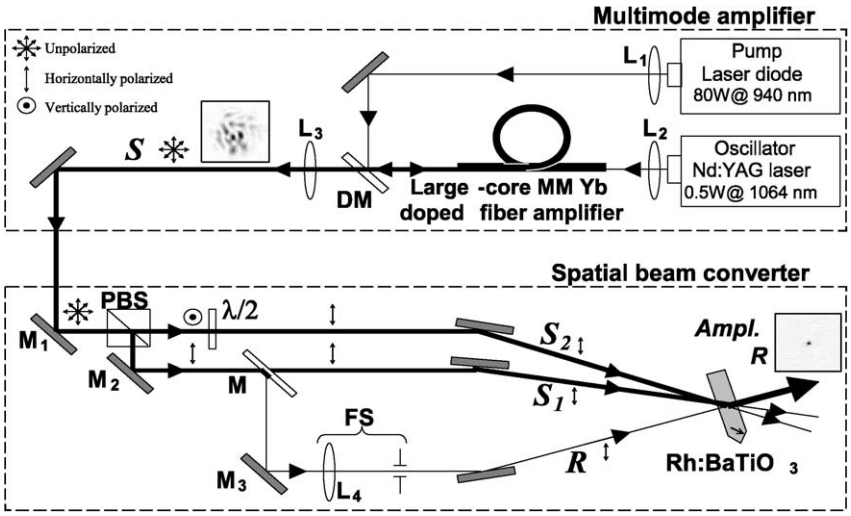

Fig. 4. Experimental setup of an Yb-doped multimode fiber amplifier with spatial beam converter. The amplified depolarized multimode signal beam S is split into its two linear polarizations and combined with an extracted singlemode beam R in a Rh:$BaTiO_3$ crystal and converted to singlemode. DM: dichroic mirror to separate 940 and 1064 nm beams. $L1, L2, L3$: lenses. $M1, M2, M3$: mirrors. $\lambda/2$: half-wave plate PBS: Polarizing Beam Splitters M: spot mirror of the size of one speckle grain of S. FS: spatial filtering device. Signal and amplified reference spot shapes are shown in squares. An arrow in the crystal indicated the c-axis orientation.
Fig. 4. Schéma expérimental d'un amplificateur à fibre multimode dopée Yb associé à un convertisseur spatial de faisceau. Le signal amplifié, dépolarisé et mutlimode S est séparé en ses deux composantes de polarisations puis combiné avec le faisceau monomode R dans un cristal de Rh:$BaTiO_3$ afin de le convertir en un faisceau monomode. DM : miroir dichroïque séparant les faisceaux à 940 et 1064 nm. $L1, L2, L3$: lentilles. $M1, M2, M3$: miroirs. $\lambda/2$: lame demi-onde PBS : Séparateur de polarisation M : Miroir point de la taille d'un grain de speckle de S. FS : filtre spatial. Les faisceaux signal et référence amplifiée sont montrés dans les carrés. Une flèche sur le cristal indique l'orientation de l'axe c.

[2] From the Institute for Physical High Technology (IPHT), Jena, Germany.

The 3.5 m long fiber absorbs a power of 60 W of the 940 nm pumping diode. The amplified signal beam S has a power of 18 W, is depolarized and bears many transverse modes as seen on picture in Fig. 4. All the speckle grains have a different elliptical polarization but are coherent with each other. A 55 μm core diameter fiber has been used in this experiment but the approach is scalable to significantly larger core diameters.

To treat its two polarizations, S is split into its two linear components S_1 (horizontal polarization) and S_2 (vertical polarization, changed to horizontal polarization by a half-waveplate, see Fig. 4). The powers of S_1 and S_2 are 8.3 W and 6.6 W, respectively. A diffraction-limited reference beam R is created by spatially selecting a small part of one of S_1 bright speckle grains with a dot mirror. This mirror is a 1 mm diameter gold spot coated on a high transmission plate. The reflected bright speckle grain is spatially filtered with a lens-pinhole system. This 110 mW reference beam R is horizontally polarized, diffraction limited and coherent with S.

S_1 and S_2 are then mixed with the reference beam R in the photorefractive crystal. In the crystal plane, R is a 1.5 mm diameter diverging beam normal to the crystal surface, and S_1 and S_2 are 1×1.5 mm^2 elliptical converging beams with a 40°incidence angle. The angle between S_1 and S_2 is 1.5°. Here, S_1 and S_2 spots are smaller than R and they overlap and amplify respectively the upper and lower halves of R. S_1 and S_2 could as well be the same size as R and overlap the whole beam.

The two-wave-mixing process in the photorefractive crystal then occurs as follows: the intensity fringes between R and S_1 are converted into a $\frac{\pi}{2}$-shifted index grating by the crystal. This grating diffracts S_1 along R and adds coherently the diffracted S_1 to R. As a result, R is amplified by S_1. The same process occurs between R and S_2. The remarkable property of this two-wave-mixing interaction is that it amplifies R intensity profile in the crystal but leaves R phase profile unchanged: S transfers only its intensity and not its phase to R.

In this self referencing interferometer, the interference pattern is very stable. The reference R is in phase with the signals S_1 and S_2, even when the temperature fluctuates in the fiber. In an early version [10], the reference beam R was taken directly on the oscillator before the amplifier. The phase fluctuations between R and S, induced by thermal and mechanical fluctuations in the fiber, had to be compensated because of the relatively slow photorefractive response. In the present article, the self referencing interferometer gets rid of this problem because R, S_1 and S_2 are always in phase and no active phase stabilization is required.

2.4. Experimental results

Under these conditions, we obtain after the spatial beam converter an amplified R output power of 11.6 W with 110 mW reference power and 14.9 W total signal power $I_S = I_{S_1} + I_{S_2}$ before the crystal. The power of S is $I_S = 18$ W at the spatial beam converter input, before M_1 in Fig. 4. Behind the crystal, the total signal is depleted to 2.7 W. Fig. 5(a) shows R power I_R versus time as it is amplified by S_1 alone, by S_2 alone, and by both S_1 and S_2. The rise time is 2 to 3 s and the two-wave-mixing power efficiencies are respectively 77, 82 and 78%. Taking into account the

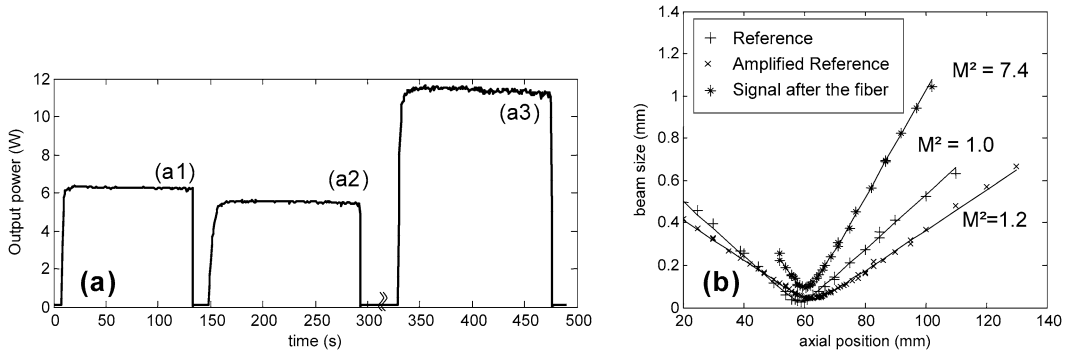

Fig. 5. Experimental results: (a) power evolution of R after the crystal (a1) with S_1 on, (a2) with S_2 on, and (a3) with both S_1 and S_2 on. The rise time (from 10 to 90% of the full power) is around 2–3 s. The base level is the power level of beam R: 110 mW; (b) measure of the M^2 parameter for the different beams. The experimental points are represented by the symbols, and the solid lines are the corresponding fitted curves.

Fig. 5. Résultats expérimentaux : (a) Évolution de la puissance de R après le cristal avec (a1) S_1, (a2) S_2, et (a3) S_1 et S_2 simultanément. Le temps de montée (de 10 à 90 % de la puissance totale) est environ 2 à 3 s. Le niveau de base est la puissance du faisceau R (110 mW), (b) Mesure du paramètre M^2 pour les différents faisceaux. Les points experimentaux sont représentés par les symboles, et les ajustements par les lignes pleines.

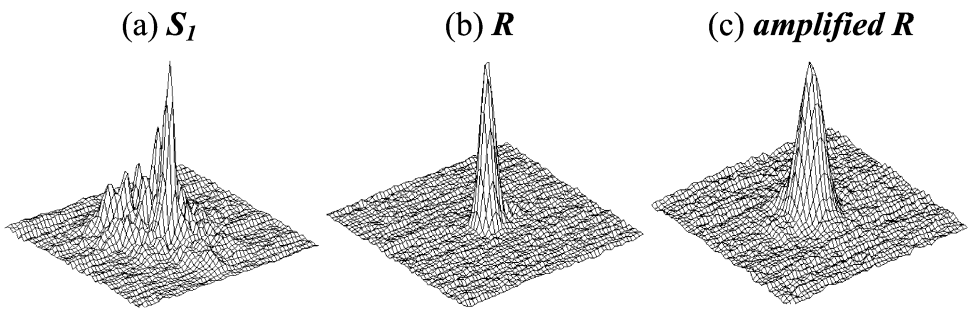

Fig. 6. Beam profiles: (a) multimode 7.4 W signal S_1 at the fiber output, (b) extracted singlemode 110 mW reference beam R, (c) singlemode 11.6 W amplified R.

Fig. 6. Profils des faisceaux : (a) signal multimode S_1 après la fibre (7,4 W), (b) référence monomode extraite R (110 mW), (c) référence amplifié dans le cristal (11,6 W).

81% transmission between the output fiber signal S and $S_1 + S_2$ before the crystal leads to a total power efficiency of 63% for the whole spatial beam converter. Of course most of these losses could be reduced by optimizing the optical elements transmission with appropriate coatings.

The M^2 parameter has been measured for the different beams with the second order moment method. The results are shown in Fig. 5(b). The reference R is diffraction limited, the 11.6 W output beam is almost diffraction limited with $M^2 = 1.2$ while S_1 is multimode with $M^2 = 7.4$. Amplified R is less diverging than R because of the additional converging thermal lens due to residual absorption in the crystal. Fig. 6 shows the intensity profiles of the waists in the far field.

After a constant illumination at 1.06 μm, we have noticed a decrease of the two-wave-mixing efficiency in the Rh:$BaTiO_3$ crystal: in Fig. 5(a), a slight decrease is visible on the 11.6 W curve. As observed in [11], depoled horizontal lines appear in the crystal with a spatial period of ≈ 190 μm. Applying a 200 mW green beam on the whole surface for several hours repoles the crystal and recovers the efficiency. This effect is similar to that reported in [11].

2.5. Scalability

Note that this beam correcting setup can be seen as a 'black box' that converts any coherent depolarized multimode beam to a diffraction limited, linearly polarized beam with the spectral characteristics of the beam emitted by the oscillator. The input beam can be highly multimode or aberrated, since the angular acceptance of the crystal is several degrees and its surface is 1 cm^2 (equivalent to a $M^2 > 1000$). The required coherence length for the multimode signal is several mm or more, corresponding to the interaction length in the photorefractive crystal. Furthermore, the concept is applicable to pulsed operation since the very large core fiber could sustain high peak power.

In conclusion, we have experimentally demonstrated that the beam issued from a multimode Yb-doped fiber amplifier can be efficiently converted into a linearly polarized and nearly diffraction limited beam. This first original MOPA architecture involves a nonlinear photorefractive mode converter allowing beam cleanup by a self-referencing two wave mixing interaction. The emitted beam has the spatial and spectral qualities of the oscillator. The achieved output power with the components used in this experiment is 11.6 W with 78% photorefractive efficiency. The important feature is that the concept can be extended to very large core fiber amplifiers which will support very high powers in the CW or pulsed regimes. Rh:$BaTiO_3$ has been used for proof of concept but alternative crystals or nonlinear mechanisms can also be appropriate for reliable operation at the high power levels required in industrial applications.

Another original MOPA architecture involving a multimode gradient-index fiber in a stimulated Brillouin scattering loop is now presented.

3. Beam cleanup in a self-aligned gradient index Brillouin cavity

In this section, we propose to accomplish beam cleanup by using the Brillouin effect in a multimode fiber. First, the theory of SBS in multimode is developed and the conditions for beam cleanup or phase conjugation to occur are isolated. We describe the experimental results that led us to the original setup using a multimode gradient-index fiber and a self-aligned loop geometry. The efficient and highly stable beam cleanup results are then described.

3.1. Theory of stimulated Brillouin scattering (SBS) in multimode fibers

Stimulated Brillouin scattering in multimode fibers can lead to phase conjugation as reported in pulsed operation [12], cw operation [13] and with a loop [14]. It can also lead to beam cleanup as observed by Bruesselbach [15] in 1993. To show that those two behaviors are linked to the fiber geometry, we calculate the Brillouin gain associated with each fiber mode in both GI and step-index (SI) fibers.

The scalar nonlinear polarization density for the Brillouin effect under the flat Brillouin gain approximation is [16,17]:

$$\mathcal{P}_{\mathrm{NL}} = \frac{3}{2}\varepsilon_0 \chi^{(3)} E_p E_p^* E_s(x, y, z, t) \tag{3}$$

with ε_0 the vacuum permittivity and $\chi^{(3)}$ the third-order nonlinearity coefficient for the Brillouin effect. $\chi^{(3)}$ is proportional to the commonly used Brillouin gain g_B. E_s and E_p are the scalar electric fields for the Stokes and the pump waves, respectively. Now consider a waveguide that can carry N modes with electric field distributions $\psi_1(x, y), \ldots, \psi_N(x, y)$ and propagation constants $\beta_1, \ldots, \beta_N$. The pump and Stokes electric fields are similarly decomposed:

$$E_{s,p}(x, y, z, t) = \sum_{i=1}^{N} c_i^{s,p}(z, t)\psi_i(x, y)\mathrm{e}^{\mathrm{i}(\pm\beta_i^{s,p} z - \omega_{s,p} t)} \tag{4}$$

where the complex mode coefficients $c_i^s(z, t)$ and $c_i^p(z, t)$ can vary along the fiber or in time. ω_s and ω_p are the Stokes and pump waves frequencies. The sign in front of β is $+$ for the pump wave and $-$ for the Stokes wave. In the following we consider the hypothesis of a scalar field (no depolarization in the guide), no absorption, no mode mixing, and cw operation (c_i^s depends only on z). Then the injection of Eqs. (4) and (3) into the well-known Maxwell propagation equations [16] leads to the following evolution equation for each Stokes mode:

$$\frac{\mathrm{d}c_n^s(z)}{\mathrm{d}z} = \alpha g_B \sum_{i,j,m} R_{ijmn} c_i^p c_j^{*p} c_m^s(z)\mathrm{e}^{\mathrm{i}\Delta\beta_{ijmn} z} \tag{5}$$

where α is a constant, R_{ijmn} is an overlapping factor, and $\Delta\beta_{ijmn}$ is a phase mismatch factor defined by Eqs. (6) and (7). After integration along the fiber, only the terms with $\Delta\beta_{ijmn} = 0$ do not vanish.

$$R_{ijmn} = \int_{-\infty}^{\infty}\int_{-\infty}^{\infty} \psi_i \psi_j^* \psi_m \psi_n^*(x, y)\,\mathrm{d}x\,\mathrm{d}y \tag{6}$$

$$\Delta\beta_{ijmn} = \beta_i^p - \beta_j^p - \beta_m^s + \beta_n^s \tag{7}$$

3.2. Phase conjugation or beam cleanup by SBS in multimode fibers?

A full resolution of Eq. (5) is possible at the Brillouin threshold for any given set of c_i^p. In the case of highly multimode fibers, it leads to good-quality phase conjugation in short SI fibers (limited to several meters by the Brillouin frequency shift [17]) and to poor-quality phase conjugation in GI fibers. Our experimental investigations in SI 50 μm and GI 62.5 μm core diameter highly multimode fibers have confirmed good-quality phase conjugation in the short (2 m) SI fiber, no phase conjugation or beam cleanup in the long (1 km) SI fiber, bad-quality phase conjugation in the short (2 m) GI fiber, and beam cleanup in the long (>30 m) GI fiber. This behavior difference between GI and SI fibers comes from the mode overlap between pump and Stokes fiber modes. In the case of SI fibers, the mode overlap factor R_{ijmn} is similar for all Stokes modes, thus enabling phase conjugation, whereas in GI fibers this factor is higher for the lower-order Stokes mode, leading to a favored reflexion of lower-order modes.

Let us try to understand where this behavior comes from. If phase conjugation occurs, the Stokes wave is the phase-conjugated replica of the pump wave, i.e., $c_i^s(0) = c_i^{p*}(0)$. Under the additional simplifying hypothesis of uniform depletion and amplification profiles [we can write $c_n^s(z) = c_n^s(0) f_s(z)$ and $c_n^p(z) = c_n^p(0) f_p(z)$ with repartition

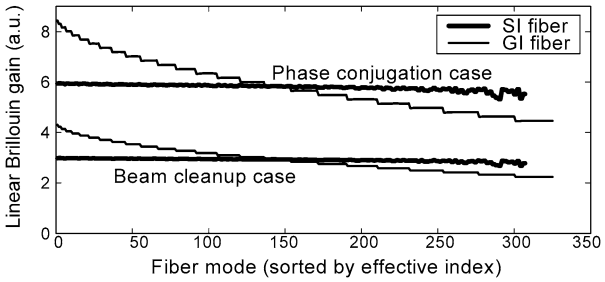

Fig. 7. Linear gain for each Stokes fiber mode sorted by propagation constants (lower order modes at the left). The calculation is done for an uniform excitation of the pump modes and for two fiber geometries: a SI fiber (normalized frequency $V = 35$) and a GI fiber ($V = 52$).

Fig. 7. Gain linéaire Brillouin de chaque mode de fibre Stokes (les modes sont triés par constante de propagation, modes d'ordre faible à gauche). Ce calcul est fait dans le cadre d'une excitation uniforme de tous les modes de pompe et pour deux géométries de fibre : une fibre SI (de fréquence normalisée $V = 35$) et une fibre GI ($V = 52$).

functions f_s and f_p independent on n] and no propagation constant degeneration (only terms with $m = n, i = j$ or $m = i, j = n$ satisfy $\Delta\beta_{ijmn} = 0$), Eq. (5) leads to the power evolution equation:

$$\frac{\mathrm{d}P_n^s}{\mathrm{d}z} = -\left(2g_B \sum_i R_{in} P_i^p - g_B R_{nn} P_n^p\right) P_n^s \tag{8}$$

with $R_{in} = R_{iinn} = R_{inin}$, $R_{nn} = R_{nnnn}$, and P_n^s and P_m^p the powers contained, respectively, in the nth Stokes mode and the mth pump mode. The power carried by each mode is $P_n(z,t) = (nc\varepsilon_0/2)|c_n(z,t)|^2$. Now in the case of beam cleanup, the Stokes wave is contained in a single fiber mode n and $P_m^s = 0$ for $m \neq n$. The power evolution, Eq. (8), is changed into

$$\frac{\mathrm{d}P_n^s}{\mathrm{d}z} = -\left(g_B \sum_i R_{in} P_i^p\right) P_n^s \tag{9}$$

The terms in parentheses in Eqs. (8) and (9) represent the linear Brillouin gain of the Stokes mode $P_n^s(z)$ and is plotted in arbitrary units at threshold in Fig. 7 for uniform repartition of pump power on fiber modes [$P_n^p(0) = P^p(0)$]. On the one hand, good-quality phase conjugation requires the same uniform repartition of Stokes power on fiber modes [$P_n^s(0) = P^s(0)$]. This condition is fulfilled in the SI fiber: the various Stokes modes experience the same linear gain, which enables high-quality phase conjugation. The condition is not fulfilled in the GI fiber, where the linear gain for the lower-order modes is nearly twice as large as for the higher-order modes: the hypothesis of phase conjugation must be rejected in the GI fiber. On the other hand, beam cleanup requires selection of a particular mode. The favored reflexion of lower-order modes in GI fibers leads to beam cleanup. In SI fibers there is no mode selection and so no beam cleanup.

In summary, we draw the following conclusions for highly multimode fibers: good-quality phase conjugation can be expected in short [17] SI fibers but not in GI fibers. Beam cleanup can be expected in GI fibers but not in SI fibers.

3.3. Experimental investigation

Experimental investigations of the Brillouin effect in a GI fiber have been carried out with the setup shown in Fig. 8. A very large core Yb-doped multimode fiber amplifier is seeded by a quasi-cw (Qcw) single-frequency laser

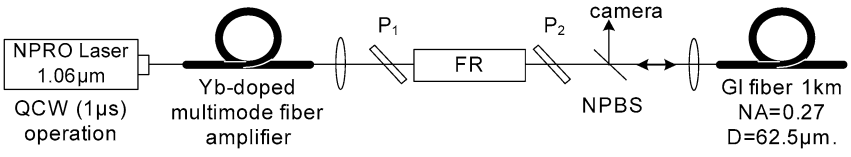

Fig. 8. Experimental setup.

Fig. 8. Schéma expérimental.

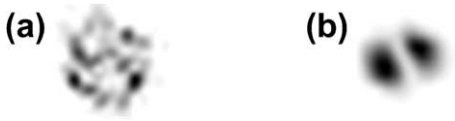

Fig. 9. Beam shapes: (a) incident pump beam, (b) reflected Stokes beam (LP_{11} mode).
Fig. 9. Faiscaux : (a) faisceau pompe incident, (b) faisceau Stokes réfléchi (mode LP_{11}).

(1 μs pulses at 33 kHz). The amplified beam is depolarized and has the shape shown in Fig. 9(a) (beam parameter $M^2 = 6.5$). Its horizontal polarization has a peak power limited to 150 W and is coupled in a 1 km long GI fiber with an aperture of NA = 0.27 and a core diameter of $d = 62.5$ μm ($V = 52$). The reflected beam is observed after the nonpolarizing beam splitter.

We observed that the Stokes beam is usually reflected as a LP_{11} mode as shown in Fig. 9(b), independently of the pump coupling conditions. The reason is that the LP_{11} mode has a more balanced overlapping with all pump modes: above threshold, pump depletion is more uniform and the LP_{11} mode gain becomes higher than the LP_{01} mode. Nevertheless, it has been possible to select the fundamental LP_{01} fiber mode with a very careful coupling of the pump beam into the lowest-order fiber modes: we then obtained a Brillouin reflectivity of 45% of the 115 W incident pump peak power in the GI fiber with a measured $M^2 = 1.2$. However, selection of LP_{01} fiber mode is difficult to obtain because LP_{11} is fundamentally favored.

To impose the LP_{01} mode to be reflected with stable operation, an external selection is required. We propose to decrease the Brillouin threshold of the LP_{01} mode by injecting part of the Stokes beam at the fiber end into the LP_{01} mode only. The Brillouin cavity is then closed for the fundamental mode and opened for higher-order modes. This design requires on the one hand, the conservation of the fundamental mode in the fiber and, on the other hand, a filter with very good rejection of the higher-order mode, especially the LP_{11} modes.

3.4. Self-aligned gradient-index Brillouin cavity setup for beam cleanup

Those two conditions are realized in our setup displayed in Fig. 10. The amplified pump pulse is coupled into the 30 m long GI multimode fiber with a core diameter of 62.5 μm and a normalized frequency $V = 52$ (325 modes on each polarization). We have observed that under careful coupling of the LP_{01} mode only, this 30 m multimode GI fiber can propagate the fundamental mode without mode mixing nor depolarization. The fundamental mode filtering is made with a singlemode fiber that is spliced to the multimode GI fiber. This 1.5 m fiber provides a complete rejection of the high order modes.

Thus only the horizontally polarized fundamental mode of the multimode GI fiber sees a closed cavity: its Brillouin threshold power is lowered and it is preferably reflected. Note that the sensitive alignment of the two fiber cores is precisely provided by the splicing.

The reason that the loop decreases the Brillouin threshold is the following. It is usually admitted that the pump power threshold P_p^{th} for the Brillouin effect without the cavity effect in fibers is defined by the empirical condition $g_B P_p^{th} L/S = 21$, where g_B is the Brillouin gain coefficient, S is the core surface, and L is the fiber length when absorption is negligible. At that pump power, the total Brillouin gain $G_B = \exp(g_B P_p^{th} L/S) = \exp(21) \approx 1.3 \times 10^9$

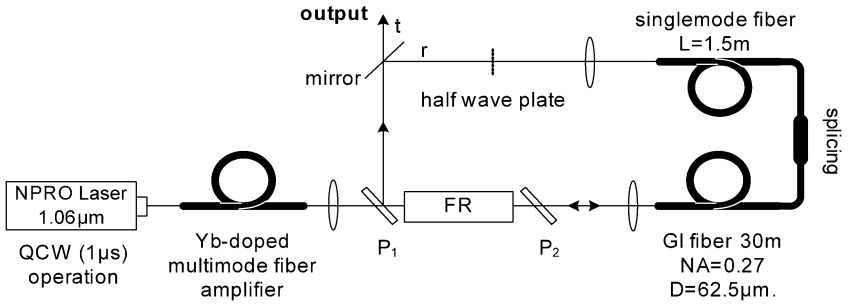

Fig. 10. Self-aligned Brillouin cavity for beam cleanup. FR: Faraday rotator, P_1, P_2: polarizing beam splitters.
Fig. 10. Cavité Brillouin auto-alignée pour beam cleanup. FR : rotateur Faraday, P_1, P_2 : séparateurs de polarisation.

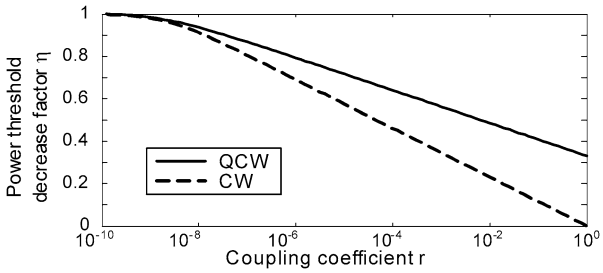

Fig. 11. Power threshold decrease in a closed Brillouin cavity relative to the open Brillouin cavity as a function of the coupling coefficient r for cw and Qcw operation.

Fig. 11. Puissance seuil dans une cavité Brillouin fermée, relativement à la même puissance en cavité ouverte, en fonction du coefficient de couplage r, et en fonctionnements cw et Qcw.

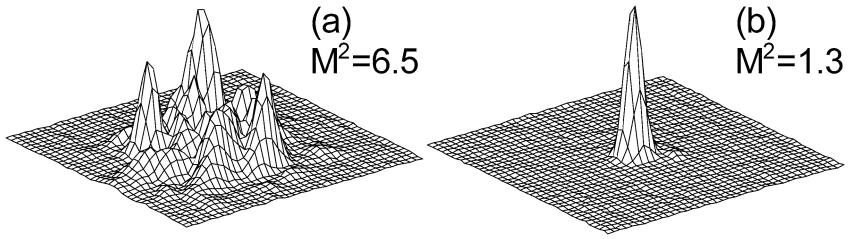

Fig. 12. (a) Pump beam shape emitted by the multimode fiber amplifier and (b) Stokes beam shapes in the far field.

Fig. 12. (a) Faisceau pompe en sortie d'amplificateur à fibre multimode, (b) Faisceau Stokes en champ lointain.

is then large enough to initiate the effect with spontaneously emitted photons at the fiber end. In the case of the Brillouin cavity, the threshold condition is reached as soon as the coupling losses are compensated by the Brillouin gain: $G_B = 1/r$, where r is the ratio of Stokes power that is injected in the singlemode fiber. The condition rewrites $g_B P_p^{th} L/S = -\ln(r)$. The power threshold is then decreased by a factor $\eta = -\ln(r)/21$. η is plotted in Fig. 11 as a function of coupling coefficient r for the case of cw regime and Qcw with three passes in the GI fiber. The spontaneous Brillouin emission is taken into account and is responsible for threshold at a low coupling coefficient of $r < 10^{-8}$. At higher coupling, the new condition implies a power threshold decrease of a factor of 3 to 5.

In the experimental setup, the coupling coefficient is $r \approx 0.2$ in Qcw regime. Power thresholds are $P_p^{th} = 39$ W with an open cavity and $P_p^{th} = 21$ W with a closed cavity. The decrease factor 0.54 is not far from the expected value 0.40. The maximum intracavity Brillouin reflectivity was 31% at 150 W of incident pump peak power in this preliminary experiment. The beam shapes of the incident pump beam and the reflected Stokes beam are shown in Fig. 12. The Stokes beam is linearly polarized and its beam quality is $M^2 = 1.3$. It is very stable and the cavity is easy to set, thanks to the precise alignment done by the splicing.

In conclusion, we have demonstrated a Brillouin cavity setup with self-alignment capacity using a standard gradient-index multimode fiber for beam cleanup of high power output of a multimode fiber amplifier. Beam cleanup is achieved by efficient reflection of the multimode beam to the fundamental gradient index fiber mode. An intracavity conversion efficiency of 31% in the fundamental mode has been obtained. Higher efficiency is expected in cw operation because of lower threshold. Further developments will include extracting the Stokes power from the cavity and recycling the vertical pump polarization. This nonlinear mode converter based on beam cleanup in a multimode GI fiber should be able to convert any coherent multimode depolarized beam into a single spatial mode linearly polarized beam with good efficiency.

4. Conclusion

We have proposed and successfully demonstrated the original approach of amplifying a beam in a very-large-core multimode fiber and restoring the beam spatial quality with nonlinear beam cleanup interactions. Two beam cleanup setups have been proposed and demonstrated:

- the self-referenced cw two-wave mixing in a photorefractive crystal at ten-watt level with good efficiency. As the photorefractive grating is built with average power only, this mode converter is expected to work in the same way with high repetition rate pulsed beam;
- the Brillouin cavity setup with self-alignment capacity using a standard gradient-index multimode fiber. Beam cleanup is demonstrated with qcw pulses. Higher efficiency is expected with cw beam and we expect to extend this scheme to short incident pulses.

The techniques demonstrated here at moderate intensities achieved a nearly 2 orders of magnitude gain in brightness (proportional to power per M^2). This schemes could be an alternative for the phasing of high power lasers and amplifiers operating in pulsed or cw regime.

References

[1] A.E.T. Chiou, P. Yeh, Optics Letters 10 (1985) 621.
[2] L. Mager, G. Pauliat, D. Rytz, M.H. Garrett, G. Roosen, Nonlinear Optics, Principles, Materials, Phenomena, Devices 11 (1995) 135.
[3] J.E. Heebner, R.S. Bennink, R.W. Boyd, R.A. Fisher, Optics Letters 25 (2000) 257.
[4] A. Brignon, J.P. Huignard, E. Lallier, Applied Physics B: Lasers and Optics 72 (2001) 789.
[5] A. Brignon, J.P. Huignard, M.H. Garrett, I. Mnushkina, Applied Optics 36 (1997) 7788.
[6] L. Lombard, A. Brignon, J.P. Huignard, E. Lallier, G. Lucas Leclin, P. Georges, G. Pauliat, G. Roosen, Optics Letters 29 (2004) 989.
[7] L. Lombard, A. Brignon, J.P. Huignard, E. Lallier, P. Georges, Optics Letters 31 (2006) 158.
[8] P. Yeh, IEEE Journal of Quantum Electronics 25 (1989) 484.
[9] N. Huot, J.M.C. Jonathan, D. Rytz, G. Roosen, Optics Communications 140 (1997) 296.
[10] L. Lombard, A. Brignon, J.P. Huignard, E. Lallier, G. Lucas-Leclin, P. Georges, G. Pauliat, G. Roosen, in: CLEO Europe 2003 Proceedings, 2003.
[11] R.S. Cudney, M. Kaczmarek, Optics Express 7 (2000).
[12] H.J. Eichler, J. Kunde, B. Liu, Optics Communications 139 (1997) 327.
[13] R.G. Harrison, V.I. Kovalev, Lu Weiping, Yu Dejin, Optics Communications 163 (1999) 208.
[14] C. Hanisch, A. Heuer, R. Menzel, Applied Physics B: Lasers and Optics 73 (2001) 851.
[15] H. Bruesselbach, in: CLEO 1993 Proceedings, 1993.
[16] R.W. Boyd, Nonlinear Optics, Academic Press, San Diego, CA, 1992.
[17] R.W. Hellwarth, Journal of the Optical Society of America 68 (1978) 1050.